THEORETICAL RESOLVING POWER OF A RADIOFREQUENCY MASS SPECTROMETER *

A. COC, R. LE GAC, M. de SAINT SIMON, C. THIBAULT, F. TOUCHARD
CSNSM-IN2P3-CNRS, Bât 108, F-91405 Orsay-Campus

1988

Abstract

Radiofrequency mass spectrometers of L.G. Smith's type can reach a resolving power of 10^6–10^7 and a precision of 10^{-9}–10^{-10}. The resolving power, shape of peaks and limitations are described. As an example, the spectrometer to be used in an experiment aimed at measuring the $\overline{p}$ $/p$ mass ratio is considered.

1 Introduction

Several successive versions of radiofrequency mass spectrometers (RFMS) were built by L.G. Smith in the sixties and with the latest[1, 2], a very high resolving power ($\simeq 10^7$)[3] and precision ($\simeq 10^{-10}$) was obtained[4]. Before his death in 1972, he performed atomic mass measurements of stable isotopes with a precision which by that time had no match[5, 6]. Meanwhile, the number and precision of mass measurements by conventional mass spectrometer have increased and measurements using cyclotron traps have been developed[7]. Recently, it was shown[8] that at least for the ^{3}H–^{3}He mass difference (relevant to $\overline{\nu}_e$ mass determination) that Smith's measurements were indeed as precise as he claimed. A new RFMS based on Smith's principle will be used for a test of CPT at CERN by comparing the charge to mass ratio of protons and antiprotons (experiment PS189). Their absolute values should be the same as according to the CPT theorem, $|q|$ and M are identical for a particle and its antiparticle. The aim of this experiment is to improve by four orders of magnitude the present upper limit on an hypothetical CPT violation in the $p-\overline{p}$ pair[9]. A very low energy (200 keV), good emittance ($\simeq 5\pi$ mm.mrad and $\Delta p/p \simeq 10^{-3}$) and reasonable intensity antiproton beam is needed and is to be developed at LEAR (CERN). In practice, the comparison will be made with H^- ions whose charge has the same sign as antiprotons. The results need to be corrected for the small mass of the two electrons (2×0.511034(14) MeV)[9] and their binding energy (13.6+0.8 eV). A 10^6 resolving power and a 10^{-9} precision is aimed at. The lower resolution compared to Smith's one is due to a compromise between resolving power and acceptance, as unlike stable isotope, antiprotons are scarce. The purpose of this article is to show how such a resolution can be obtained. In practice, one has to cope with non linear effects which must be minimized. They are neglected here but will be treated in forthcoming papers as they depend on details of the apparatus which cannot be presented here. However, the main contributions will be reviewed in section 6. The ideas for calculating the resolving power of such a mass spectrometer are scattered in references [1] and [2], but the formula giving the resolving power of the most performant design appeared nowhere.

*Nucl. Instr. and Meth. **A271** (1988) 512–517

2 Bases of the RFMS

In a conventional mass spectrometer, the trajectories of two different ions A and B are identical when all the voltages U obey the relation $M_A \times U_A = M_B \times U_B$ where M is the ion mass. Once the trajectories have been made identical, the measurement of the ratio of the applied voltages lead to the ratio of masses. However, practically, the accuracy on a relative voltage determination does not exceed 10^{-7}. It is thus unrealistic to intend to increase the accuracy beyond this value by increasing the resolving power of such spectrometers. The physical characteristic which can be measured with the highest accuracy (10^{-14}) is frequency. The (cyclotronic) motion of a charged particle inside a static and homogeneous magnetic field provides the necessary connection between mass and frequency. This (cyclotron) frequency is given classically by $\omega_c = qB_0/M$. If the magnetic field is stable enough, the frequencies and masses of the two ions obey a relation $M_A \times \omega_A = M_B \times \omega_B$ similar to the one relating masses and voltages

3 Principle of the spectrometer

The main parts of the spectrometer consist of a magnet with a highly homogeneous field, a four-fold radiofrequency cavity (modulator), and 2 symmetrical lines for the injection and ejection of the beam (Fig. 1). The beam is injected into the homogeneous area of the magnetic field by an electrostatic

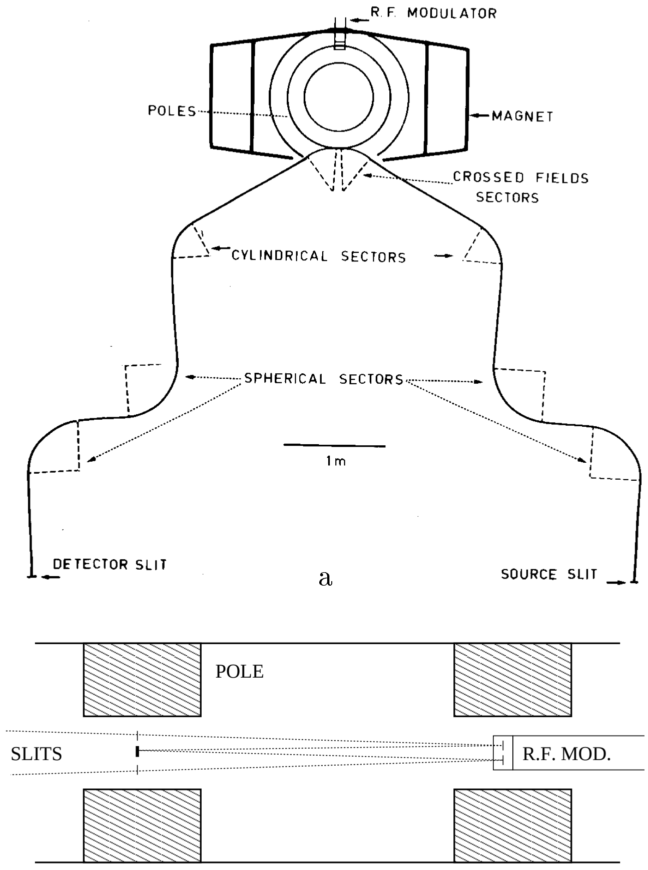

Figure 1: General scheme of the radiofrequency mass spectrometer (a) and vertical cut view of the magnet (b) showing the nominal trajectory and the various slits.

cylindrical deflector which is the last element of the injection line. It makes two turns inside the magnet and is ejected by a second deflector. At the end of the first and third half-turn, it crosses the modulator. The modulation frequency ω is adjusted so that the accelerating electric field has opposite phases for the two crossings. In these conditions, the final acceleration (after the two turns) is null. The electrostatic injecting and ejecting lines act as energy filters which have to be tuned to the same value T_0 of the kinetic energy. The lines have a unit linear magnification and a high dispersive power in energy A_δ. The injection line creates an image of the object slit at the entrance of the magnet and on the first modulator slit. Symmetrically, the ejection line creates the image of the second modulator slit in the plane of the detector slit. Inside the magnet, horizontal focusing is obtained naturally after each half-turn (Fig. 2). The transmission will hence be maximum when the phase condition is

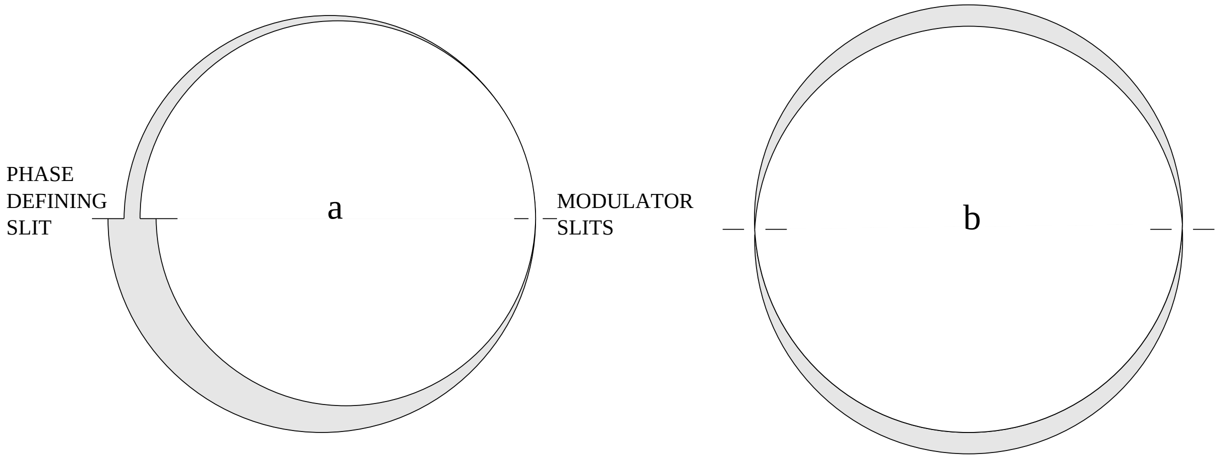

Figure 2: Horizontal cut view of the beam within the magnet showing the energy focusing at each turn and the effect of the phase defining slit (a) and the angular focusing at each half-turn (b).

fulfilled which, as we will see occurs when ω/ω_c is a half-integer. Inside the magnet, the ions follow an helicoidal trajectory with mean radius $R_0 = \sqrt{2MT_0}/qB_0$. The beam is injected above the median plane of the magnet with a small dip angle. This insures that the injection and ejection (below the median plane) are separated in height (Fig. 1b)

4 Resolving power of the RFMS

The acceptance of the spectrometer can be factorized into a geometrical part and a modulation dependent part. This last factor is 1 when no modulation is applied and its variation with ω determines the shapes of the peaks.

4.1 Principle

Depending on the phase ωt of the electric field, an ion is acc/decelerated when it crosses the modulator and its energy is changed by $T_m \sin \omega t$. The properties of the magnetic field ensure that after one turn, the beam is focused in energy and angle (Fig. 2) on the second slit of the modulator. After the two crossings, one has :

$$\Delta T = T_m \sin \omega t + T_m \sin(\omega(t + 2\pi/\omega_c))$$

i.e.

$$\Delta T = 2T_m \sin(\omega t + \pi\omega/\omega_c) \cos(\pi\omega/\omega_c) \tag{1}$$

If $\omega = (n + 1/2)\omega_c$, where n is an integer, $\cos(\pi\omega/\omega_c)$ is null and so is ΔT whatever t is. The transmission is maximum as the lines filter the ions whose energy remains unchanged. When the frequency ω is scanned, peaks are observed for every integer value of $\omega/\omega_c - 1/2$. The higher the energy resolution of the two lines and the faster ΔT changes with respect to $dM/M = -d\omega_c/\omega_c$, the higher is the mass resolving power of the spectrometer. (It is convenient to consider the mass M instead of ω as a variable to determine the resolving power).
Near to the center of a peak ($\omega/\omega_c \simeq n + 1/2$) and taking the first order expansion of equation 1 with respect to ω_c one has :

$$\Delta T \simeq 2\pi n T_m \cos(\omega t)\Delta\omega_c/\omega_c \tag{2}$$

Hence, in order to improve the peak shape, the phase must be limited so that $|\cos\omega t| \simeq 1$. This is achieved by the"phase defining slit" situated halfway between the two passages through the modulator (Fig. 2b). If w is the common width of the slits (the phase defining slit excepted), T_0 the kinetic energy and A_δ the dispersive power in energy of the lines, the selectivity in energy is $\Delta T/T_0 \simeq w/A_\delta$ and using equation 2 one obtains :

$$\Delta M/M \simeq (2\pi n)^{-1}(T_0/T_m)(w/A_\delta) \tag{3}$$

This formula is indeed the FWHM resolving power of the RFMS as it will be shown in the following.

4.2 Phase defining slit

The modulation of the orbit diameter is $D(t) = 2R_0 + D_m \sin\omega t$ with $D_m = R_0 T_m/T_0$, the small amplitude of this modulation. D_m is important to determine the extension of the beam inside the magnet where the field has to be sufficiently uniform and is also related to the phase defining slit width $w_\Phi \gg w$. The position of an ion relative to the phase defining slit axis is then $D_m \sin\omega t$ as it is situated halfway between the two passages through the modulator. This slit limits the phase in such a way that $|D_m \sin\omega t| < w_\Phi/2$. The acceptance in phase is then $[-\Phi_0, \Phi_0] \cup [\pi - \Phi_0, \pi + \Phi_0]$ where $\Phi_0 = \arcsin(w_\Phi/2D_m)$. Typically, $\Phi_0 = \pi/6$, $|\cos\omega t| > 0.87$ and the transmission is reduced by a factor $2\Phi_0/\pi = 1/3$.

4.3 Image displacement

Since the peaks shape is determined by the displacement of the image of the object slit in front of the detector slit, it is better to make it appear.
Due to the symmetry of the whole spectrometer, the horizontal linear magnification is unity and the energy dispersive power is null between the object and detector slits (but not between the modulator and detector slits where it is $A_\delta \gg R_0$). The image of the object slit is displaced in the detector slit plane by the quantity $A_\delta \Delta T/T_0$ for small values of the energy change $\Delta T/T_0$ induced by the modulator. One may also introduce $D'_m = A_\delta T_m/T_0$ which is related to D_m by $D'_m = D_m A_\delta/R_0$.
x_{obj}(resp. x_{det}) is the horizontal position of an ion passing the object (resp. detector) slit where the origin is taken at the center of the slit. To cross both slits it must have $|x_{\text{obj}}| \leqslant w/2$ and $|x_{\text{det}}| \leqslant w/2$. According to the above mentioned optical properties of the spectrometer and equation 2 or 3, one has in the vicinity of the peaks:

$$\Delta x = x_{\text{det}} - x_{\text{obj}} = \mp 2\pi n D'_m \Delta M/M \tag{4}$$

The phase defining slit ensures that $\cos\omega t \simeq \pm 1$ in equation 2. The two possible signs of the cosine show that the image of the objet slit is twofold unless the total modulation is null. When it is different from zero the two images are displaced symetrically with respect to the axis of the detector slit. If the images and detector slits have the same width (unit magnification), the shape of the peaks is triangular. More precisely, relative to the maximum ($\Delta x = 0$), the transmission is halved when ω/ω_c is such that $|\Delta x| = w/2$, i.e. $w/2 = 2\pi n D'_m |\Delta M/M|$ and

$$\mathcal{R}^{-1} = (\Delta M/M)_{\mathrm{FWHM}} = (2\pi n)^{-1}(w/D_m)(R_0/A_\delta) \quad (5)$$

The shape of the peaks is represented in figure 3. Between the "normal" peaks, small and broad peaks are observed. Their nature will be described in the next chapter, however they are of no practical interest. Actual peaks obtained by L.G. Smith can be seen in reference [2].

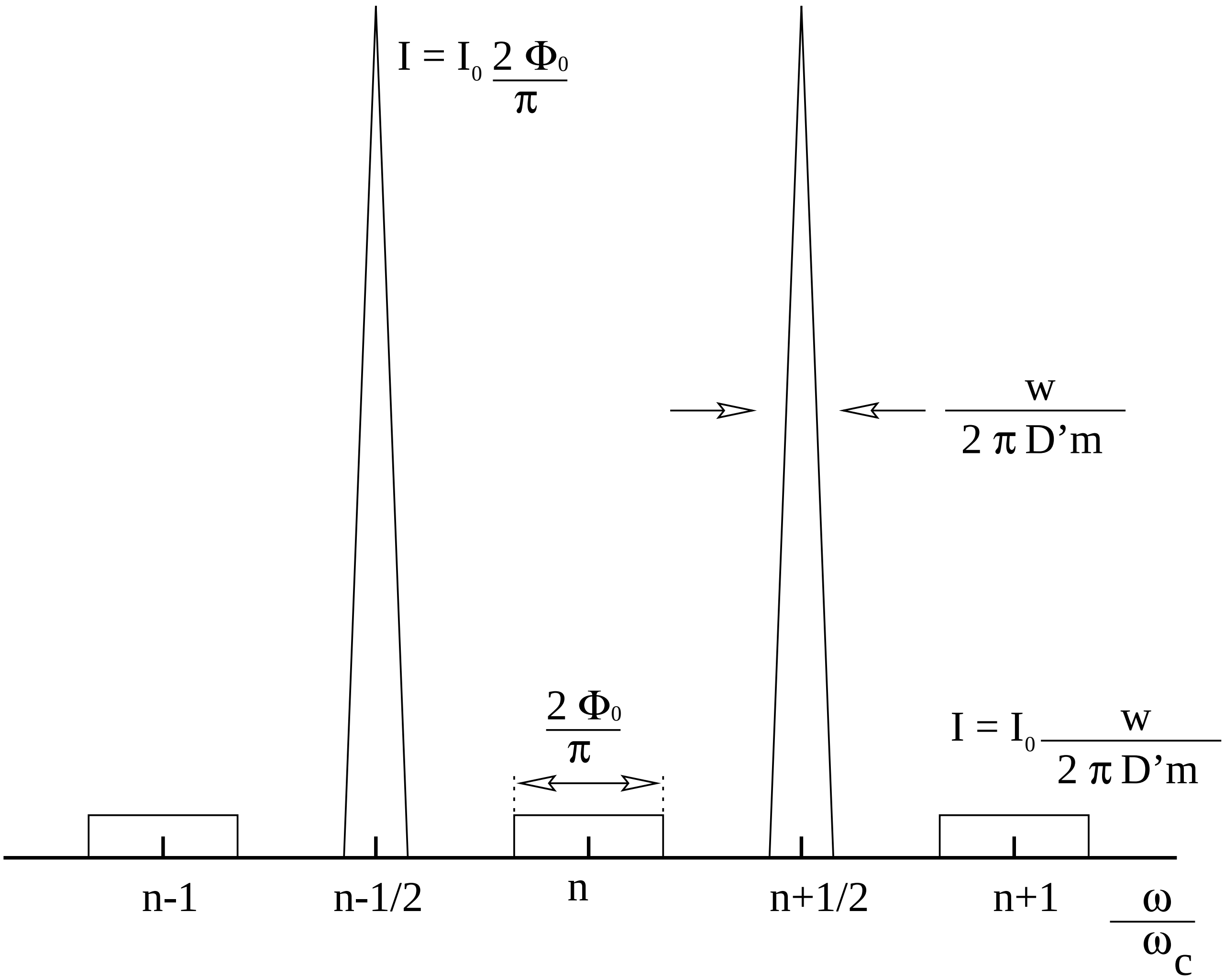

Figure 3: Shape of the integer and half-integer peaks (see text)

Using the numerical values of reference [11], i.e. $n = 1500$, w=0.2 mm, $D_m = 5$ mm, $R_0 = 500$ mm, $A_\delta = 3800$ mm, one obtains $\mathcal{R} \simeq 1.8 \times 10^6$ for the PS189 mass spectrometer. However, practically, the resolving power will be somewhat smaller as it is explained in section 6.

5 Geometrical interpretation

The principle of the RFMS may be viewed more conveniently using Fresnel's diagrams representing the sum of the two modulations. In the following, $\Delta\omega_c/\omega_c$ need not be small as in the preceding section. The sum of the two modulation can be written as

$$x_{\mathrm{det}} = x_{\mathrm{obj}} + D'_m \sin\omega t + D'_m \sin(\omega t + \Phi) \quad (6)$$

where $\Phi = 2\pi(\omega/\omega_c - n)$ can take any value between 0 and 2π.
The time dependence of the phase is represented by ωt while Φ represents the relation between the radiofrequency ω and the cyclotron frequency ω_c (the peaks occur for $\Phi = \pi$). The result of the two modulations is represented by the sum of the vectors of polar coordinates $(D'_m, \omega t)$ and $(D'_m, \omega t + \Phi\ )$ (Fig. 4). The projection of this sum on the x axis gives the change in x after two turns : $x_{\text{det}} - x_{\text{obj}}$.

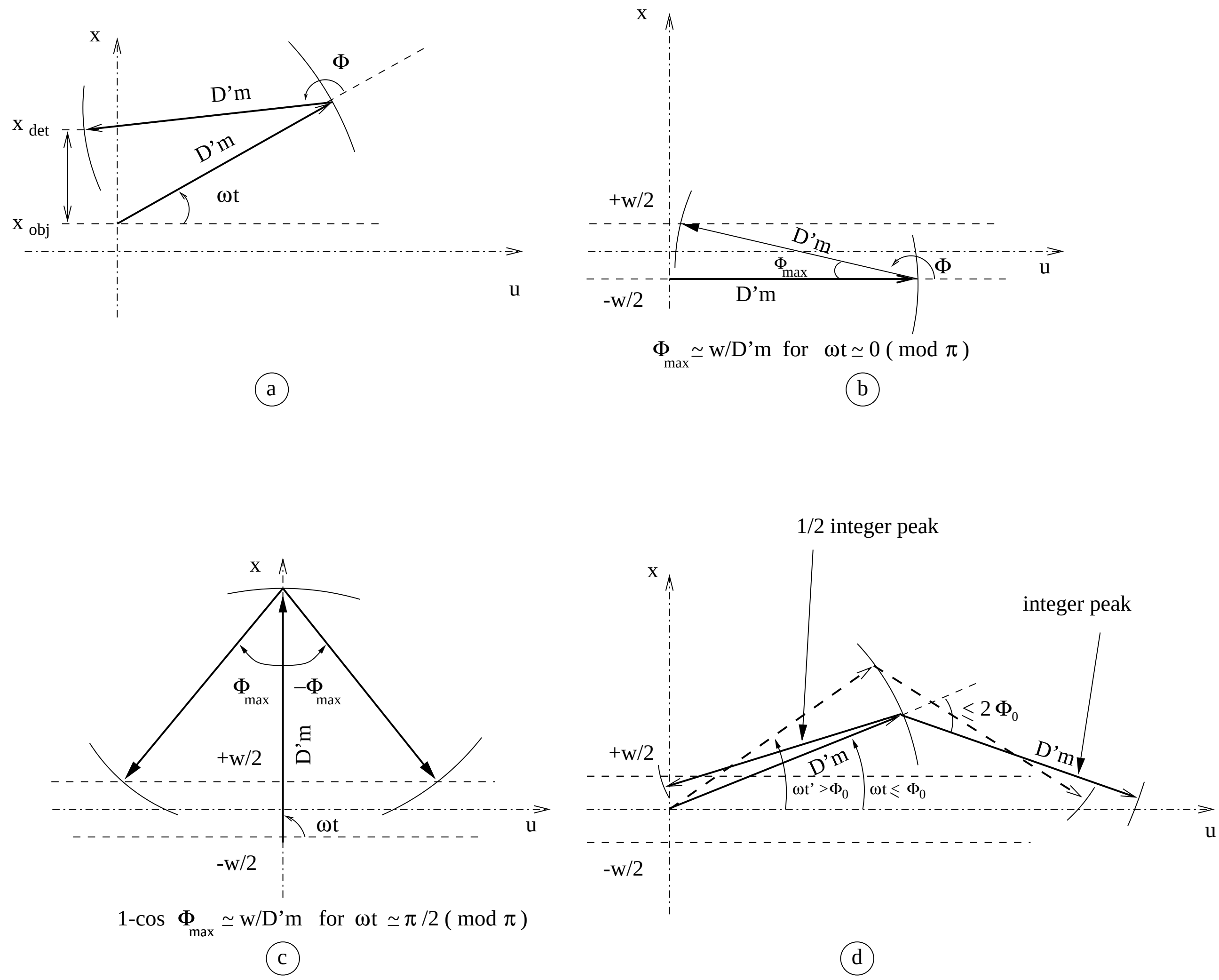

Figure 4: A Fresnel diagram is convenient to represent the sum of the two modulations (a). The projection onto the x axis gives the displacement of the image. Two extreme cases are depicted in (b) and (c), the second is suppressed by the phase defining sli. In (d) are displayed the diagrams which are related to the integer and half-integer peaks.

The resolving power and the transmission as a function of ω are related to the range in Φ for which an ion crosses both slits. Figures 4b and 4c depict two extreme cases where $\omega t = 0$ and $\pi/2$. When $\omega t = 0 \pmod{\pi}$, this condition is fulfilled when $|\Phi - \pi| \leqslant w/D'_m$ but when $\omega t = \pi/2 \pmod{\pi}$, the constraint is weaker : $|\Phi - \pi| \leqslant \arccos(1 - w/D'_m)$. As w/D'_m is small ($\simeq 0.01$), the diagram of Figure 4c contributes only to the broadening of the peaks. As it has already been mentioned, this effect is eliminated by the phase defining slit. Figure 4d shows that for any value of Φ , there is a limited range of ωt for which the sum of the two modulations is approximately zero even if $\Phi \neq \pi$. Consequently the transmission never drops to zero between two peaks. The phase defining slit eliminates this effect in the vicinity of the half-integer ($\Phi = \pi$) peaks but not in the region around $\Phi = 0$ (i.e. $\omega/\omega_c = n$)

where broad and small (integer) peaks are observed. However, they are not disturbing as they are far from the interesting ones. Thanks to the phase defining slit, the half-integer peaks are limited in width by $|\Phi - \pi| \leqslant |cos\Phi_0|^{-1} w/D'_m$

The approximate value of the width $2\Phi_0/\pi$ and height $w/(2\pi D'_m) = (w/D_m)(R_0/A_\delta)/2\pi$ of the integer peaks can be readily obtained from figure 4. For instance, the height is given by the ratio of the allowed range of ωt (mod 2π), namely $2w/2D'_m$ divided by the total range 2π (mod 2π). However figure 3 shows that they cannot be used due to the large value of their width.

6 Effects limiting the resolving power

Here are summarized the main effects limiting the resolving power. More details can be found in reference [11], and other articles are in preparation.

6.1 Relativistic effect

What we are interested in is obviously the rest mass M_0. However in the case of $\overline{p}$ (and light ions) what is really measured is the relativistic mass as the kinetic energy cannot be neglected since $T_0/M_0 \simeq 2 \times 10^{-4}$. The cyclotron frequency is still given by the same formula $\omega = qB/M$ but M represents the relativistic mass. It is the sum of the rest mass and the kinetic energy after the first passage through the modulator : $M = M_0 + T_0 + T_m \sin \omega t$. This has two consequences : the kinetic energy must be known precisely and the relativistic "modulation" of the mass contributes to the broadening of the peaks. However, this effect can be compensated by a small radial gradient in the otherwise homogeneous magnetic field.

6.2 Effect of the inhomogeneities of the magnetic field

Our goal is to obtain a resolving power of 10^6, but it does not mean that the magnetic field inhomogeneities have to be smaller than 10^{-6}. Intuitively the relevant quantity is some kind of average value of the magnetic field along the trajectory. More precisely, the change δ_τ of the period τ_c ($\tau_c \omega_c = 2\pi$) induced by the difference between the real field $\vec{B}(\vec{r})$ and the ideally homogeneous field $\vec{B}_0$ is given by [12]

$$\delta\tau \simeq (R_0 B_0)^{-1} \times \int_0^\tau c(\vec{R}_0(t) - \vec{R}_0(0)|\vec{e}_y|\vec{B}(\vec{R}_0(t)) - \vec{B}_0)dt$$

where $\vec{R}_0(t)$ is the trajectory in the ideal field $\vec{B}_0$ for given initial conditions. $\vec{e}_y$ is a unit vector normal to the symmetry plane of the modulator and $(|\ |)$ denotes the scalar triple product (i.e. the determinant of the components of the three vectors). When varying the initial conditions within the acceptance, the relative variation $\delta^2\tau/\tau_c$ should be less than 10^{-6} to avoid spoiling the resolving power of the RFMS. The effect of the inhomogeneities can be reduced using electric shim coils [11] These coils can also be used to create a small radial gradient which induces an effect proportional to the modulation ωt like the relativistic mass modulation. This last effect can then be compensated by a radial gradient of appropriate value.

6.3 Effect within the modulator

Several effects are linked to the modulator. During the finite acceleration time, the ion does not follow a pure cyclotronic motion. This effect, like the relativistic one, is proportional to the modulation and can be compensated as explained above. The electric field in the cavities must be identical ($\simeq 10^{-3}$) in the upper (modulation) lower (demodulation) cavities and along the slits. The modulation efficiency of the modulator depends upon the energy of the ion. Hence, the effect of the demodulating cavities is slightly different from that of the modulating ones. This effect is clearly of the second order of the modulation amplitude.

6.4 Effect of the optical aberrations

This problem is common to any mass spectrometer, but in our case there are a few differences. The slits are rather wide compared to the scale of the spectrometer ($w/R_0 \simeq 4 \times 10^{-4}$) but we aim at a large acceptance. Not only at the detector slit the aberrations have to be minimized but also at modulator slits. The exit line has to cope with the large residual energy modulation. These effects increase the width of the images by up to 30%.
Considering the above mentioned limitations the effective resolving power should be $\mathcal{R} \approx 10^6$.

7 Effects limiting the precision

The frequency ω of the modulation will be scanned by discrete values ω_i around the resonance and the number N_i of transmitted ions recorded. The value of ω at resonance will be determined as the centroid (first moment) of the measured distribution :

$$\omega = \sum_i N_i \omega_i / N \tag{7}$$

with $N = \sum N_i$.
The absolute values of the mass of the antiproton, magnetic field, are known a priori with a precision $\simeq 10^{-5}$ sufficient to determine the integer value $n = \mathrm{Int}(\omega/\omega_c)$ without ambiguity. From the relation $\omega = \omega_c(n + 1/2)$ one deduces that $|dM/M| = d\omega_c/\omega_c = d\omega/\omega$ as there is no "error" on n. The uncertainty on the determination of the centroid will then be given by the variance σ of the distribution :

$$\sigma^2 = \sum_i N_i(\omega_i - \omega)^2/N$$

For a triangular peak, the ratio FWHM/σ=2.45. The accuracy on the determination of the centroid can be expressed as the product of two terms :

$$\frac{dM}{M} = \frac{d\omega}{\omega} = \frac{\sigma}{\omega}\frac{d\omega}{\sigma} = \mathcal{R}^{-1}\frac{d\omega}{2.45\sigma}$$

The first term is the inverse of the resolving power of the spectrometer at half maximum which is expected to be 10^6. The second term depends on statistics. If the background is negligible, one obtains $d\omega/\sigma = 1/\sqrt{N}$. In order to reach 10^{-9} for dM/M, it is thus necessary to accumulate enough statistics to obtain $d\omega/\sigma < 2.5 \times 10^{-3}$, i.e. $N > 2 \times 10^5$. However,this is not necessarily sufficient since it is here assumed that the statistics is the only limiting factor and one has to check that it is actually the case. The main parameters to look at are a priori the stability of the magnetic field, the influence of the energy selection and that of the modulation amplitude.

Acknowledgements

We thank A.H. Wapstra and E. Koets for the many fruitful discussions we had about the L.G. Smith spectrometer when we started this project. We are grateful to R. Fergeau from CSNSM, H. Haebel (design phase), H. Herr, G. Lebée, G. Petrucci and G. Stefanini from CERN who collaborated with us in the design and construction of the spectrometer based on the principles exposed in this article and whose contributions were essential. We are especially indebted to R. Klapisch who initiated this experiment and whose encouragements never failed during the subsequent phases of its realization.

References

[1] L.G. Smith Proc. Int. Conf. on Nuclidic Masses, ed. H. E. Duckworth (Univ. of Toronto Press, Toronto, Canada, 1960) p.418

[2] L.G. Smith, Proc. 3rd Int. Conf. on Atomic Masses, ed. R. C. Barber (Univ. of Manitoba Press, Winnipeg, Canada, 1967) p.811

[3] E. Koets, J. Phys. **E** : Sci. Instr. 14 (1981) 1229

[4] L.G. Smith, Phys. Rev. **C**4 (1971) 22

[5] L.G. Smith and A.H. Wapstra, Phys. Rev. **C**11 (1975) 1392

[6] L.G. Smith, E. Koets and A.H. Wapstra, Phys. Lett. **B**102 (1981) 114

[7] E.T. Lippmaa, R.I. Pikver, E.R. Suurmaa, Ya.O. Past, Yu.K. Puskhar, I.A. Koppel and A.A. Tammik, JETP Lett. 39 (1984) 646

[8] G. Audi, R.L. Graham and J.S. Geiger, Z. Phys. **A**321 (1985) 533

[9] Review of Particle Properties, Phys. Lett. **B**170 (1986)

[10] A.H. Wapstra and G. Audi, Nucl. Phys. **A**432 (1985) 1

[11] A. Coc, R. Fergeau, C. Thibault, M. de Saint Simon, F. Touchard, E. Haebel, H. Herr, R. Klapisch, G. Lebée, G. Petrucci and G. Stefanini, Int. Rept. LRB 85-01, CSNSM, Orsay (1985).

[12] A. Coc, PS189/CERN/88-01 Note